

High-frequency Isotope Compositions Reveal Different Cloud-top and Vertical Stratiform Rainfall Structures in the Inland Tropics of Brazil

V. Santos¹, A. M. Durán-Quesada² and R. Sánchez-Murillo³, D. Gastmans¹

¹São Paulo State University (UNESP), Environmental Studies Center. Av. 24A, 1515, Bela Vista, 13.506-900, Rio Claro (SP), Brazil.

²Escuela de Física; Centro de Investigación en Contaminación Ambiental; Centro de Investigaciones Geofísicas, Universidad de Costa Rica, San José 11501, Costa Rica.

³Tracer Hydrology Group, Department of Earth and Environmental Sciences, University of Texas at Arlington, Arlington, Texas 76019, USA.

Corresponding author: Vinicius dos Santos (vinicius.santos16@unesp.br)

Key Points:

- Weather systems and cloud development modulate rainfall isotope depletions.
- Cloud top temperature, cloud area, and water content (liquid-ice ratio) are key parameters to decipher tropical rainfall isotope variations.
- Isotopic variations during intra-evens are controlled by cloud-top temperature variations, rainfall vertical structure, and the height of the melting layer.

Abstract

Understanding the key drivers controlling rainfall stable isotope variations in inland tropical regions remains a global challenge. We present novel high-frequency isotope data (5-30 minute intervals) to disentangle the evolution of six stratiform rainfall events (N=112) during the passage of convective systems in inland Brazil (September 2019-June 2020). These systems produced stratiform rainfall of variable cloud features. Depleted stratiform events ($\delta^{18}\text{O}_{\text{initial}} \leq -4.2\text{‰}$ and $\delta^{18}\text{O}_{\text{mean}} \leq -6.1\text{‰}$) were characterized by cooler cloud-top temperatures ($\leq -38\text{°C}$), larger areas ($\geq 48\text{ km}^2$), higher liquid-ice ratios (≥ 3.1), and higher melting layer heights ($\geq 3.8\text{ km}$), compared to enriched stratiform events ($\delta^{18}\text{O}_{\text{initial}} \geq -3.8\text{‰}$ and $\delta^{18}\text{O}_{\text{mean}} \geq -5.1\text{‰}$). Cloud vertical structure variability was reflected in a wide range of $\delta^{18}\text{O}$ temporal patterns and abrupt shifts in d -excess. Our findings provide a new perspective to the ongoing debate about isotopic variability and the partitioning of rainfall types across the tropics.

Plain Language Summary

In this study, we use water isotopes to understand the formation of stratiform rainfall in the inland tropics of Brazil. Meteorological information from satellite products and micro rain radar vertical observations was used to analyze isotopic patterns at high-resolution (5-30 minute intervals). Our results revealed that stratiform clouds with higher cloud-top temperature, produced rainfall events enriched in heavy isotopes (developed stage with a consolidated melting layer), while colder clouds in dissipation stages and with unconsolidated melting layers produced rains depleted in heavy isotopes. Our findings provide a detailed isotope and vertical cloud structure framework to improve isotope-enabled model parametrization across the inland tropics.

1 Introduction

Sub-daily isotope compositions ($\delta^{18}\text{O}$ - $\delta^2\text{H}$) have been extensively used for the analysis of precipitation events and their association with the origin and transport of water vapor, precipitation formation and types, cloud vertical structure, the evolution of synoptic-scale systems, and cloud base processes (Aemisegger et al., 2015; Celle-Jeanton et al., 2001; S. D. Gedzelman & Lawrence, 1990; T. Han et al., 2020; Muller et al., 2015). Studies using high-frequency sampling schemes have highlighted the relevance of convective and stratiform rainfall types in controlling isotope ratios during extreme events, such as organized mesoscale convective systems (Munksgaard et al., 2020; Srivastava et al., 2012; Sun et al., 2019), squall lines (Landais et al., 2010; Camille Risi et al., 2010; Tremoy et al., 2014), and cyclones (X. Han et al., 2021; Sánchez-Murillo et al., 2019; Xu et al., 2019).

Commonly, convective systems in the inland tropics of Brazil generate both convective and stratiform rainfall. The occurrence of these systems can be simultaneous or present a temporal lag. The stratiform rainfall area (or fraction) is characterized by weaker vertical air motions ($\pm 1\text{ m s}^{-1}$), radar echoes showing weak horizontal gradients, and clear bright bands (in most cases). Such conditions favor rainfall generation with predominant low rain rates (5 mm h^{-1}), longer duration (1-3 hours), and large spatial distribution ($\sim 100\text{ km}$) (Houze, 1989, 1997; Schumacher & Houze, 2003).

Here, we hypothesize that isotope patterns in stratiform rainfall in the inland tropics of Brazil are controlled by differences in cloud-top and cloud structure during the various stages of the life cycle of cloud systems. Therefore, we used high-frequency isotope data (5-30 minute intervals) from Rio Claro, Sao Paulo, Brazil to evaluate the role of cloud vertical structure and

weather systems in controlling the isotopic variability of stratiform rainfall. Our findings provide observational evidence on the evolution and development of stratiform rainfall and contribute to understanding the spatio-temporal dynamics of cloud microphysical processes and their relationship with surface isotopic compositions. Similarly, our results highlight the relevant role of precipitation types (e.g., stratiform versus convective; Aggarwal et al., 2016) on the resulting rainfall isotope compositions in the tropics (Munksgaard et al., 2019).

2 Materials and Methods

2.1 Rainfall sampling and isotopic analysis

High-frequency rainfall samples were collected from September/2019 to June/2020 at the Rio Claro station (code: 837470, -22.39 °S, -47.54 °W, 670 m asl) located at the Environmental Studies Center – São Paulo State University (CEA-UNESP). Rainfall was collected using a passive sampler at 5, 10- or 30-minute intervals, depending on rainfall intensity and the volume required for isotopic analysis. Each rain sample was filtered using a 0.45 µm cellulose acetate syringe filter and immediately transferred and stored in 20 mL HDPE vials at 5 °C until analysis. In total, 112 samples were collected during six stratiform events.

Rainfall samples were analyzed for stable isotope composition using Off-Axis Integrated Cavity Output Spectroscopy (Los Gatos Research Inc., USA) at the Hydrogeology and Hydrochemistry laboratory of the Department of Applied Geology (UNESP – Rio Claro, Brazil) and the Chemistry School of the National University (UNA, Heredia, Costa Rica). All results were expressed in per mil (‰) relative to Vienna Standard Mean Ocean Water (V-SMOW). The certified calibration standards used in UNESP were USGS-45 ($\delta^2\text{H} = -10.3$ ‰, $\delta^{18}\text{O} = -2.24$ ‰), USGS-46 ($\delta^2\text{H} = -236.0$ ‰, $\delta^{18}\text{O} = -29.80$ ‰), including one internal standard (Cachoeira de Emas - CE – $\delta^2\text{H} = -36.1$ ‰, $\delta^{18}\text{O} = -5.36$ ‰). USGS standards were used to calibrate the results on the V-SMOW2-SLAP2 scale, whereas CE was used for memory and drift corrections. At UNA, the certified standards MTW ($\delta^2\text{H} = -130.3$ ‰, $\delta^{18}\text{O} = -16.7$ ‰), USGS45 ($\delta^2\text{H} = -10.3$ ‰, $\delta^{18}\text{O} = -2.2$ ‰), and CAS ($\delta^2\text{H} = -64.3$ ‰, $\delta^{18}\text{O} = -8.3$ ‰) were used to correct the measurement results for memory and drift effects and to calibrate them on the V-SMOW2-SLAP2 scale (García-Santos et al., 2022). The analytical uncertainty (1σ) was 1.2 ‰ for $\delta^2\text{H}$ and 0.2 ‰ for $\delta^{18}\text{O}$ for UNESP analysis and 0.38 ‰ for $\delta^2\text{H}$ and 0.07 ‰ for $\delta^{18}\text{O}$ for UNA analysis (García-Santos et al., 2022). The deuterium excess (d -excess) was calculated as: $d = \delta^2\text{H} - 8 \cdot \delta^{18}\text{O}$ (Dansgaard, 1964). This second-order parameter was used to analyze the influence of moisture recycling and transport (Froehlich et al., 2002; Jouzel et al., 2013) and potentially evaluate the occurrence of kinetic fractionation in low-humidity conditions during below-cloud evaporation (Aemisegger et al., 2015; Graf et al., 2019).

2.2 Meteorological measurements

Meteorological data were recorded at one-minute intervals using a Decagon Automatic Weather Station (AWS) Em50 including rain rate (ARR, mm), temperature (T, °C), relative humidity (RH, %), pressure (P, kPa). The Lifting Condensation Level (LCL, m) was computed using AWS RH and T data following Soderberg et al (2013): $\text{LCL} = (T - T_{\text{dew}}) / (\Gamma_d - \Gamma_{\text{dew}})$, where T (°C) is the ambient temperature, T_{dew} (°C) is the dewpoint temperature, Γ_d (°C) is the dry adiabatic lapse rate, and Γ_{dew} (°C) is the wet adiabatic lapse rate (Soderberg et al., 2013).

Reflectivity (Z, dBZ), fall velocity (w , m s^{-1}), liquid water content (LWC, g m^{-3}), and radar rain rate (Rrr, mm) were obtained from a Micro Rain Radar (MRR) (MRR-2 – METEK). The MRR data collection was programmed at a frequency of 24.230 GHz with a modulation of 0.5 – 15 MHz. This study tested different height resolutions in a range bin of 31: 150 m, 200 m, 300 m, and 350 m. As a result of this testing, the vertical profiles selected were 4,650 m, 6,200 m, 9,300 m, and 10,850 m. MRR parameters were used to investigate the rainfall vertical structure and its correlation with the surface isotopic compositions. The MRR data analysis provides a good representation of the cloud vertical structure (Endries et al., 2018; Mehta et al., 2020; Muller et al., 2015). The mean values of Z, w , Rrr, and LWC near the surface and at altitude were used to characterize the local meteorological conditions, delimit the melting layer and identify the bright band (BB). The identification of BB was employed for the definition of stratiform rainfall, following the commonly used radar-based rainfall categorization (Endries et al., 2018; Houze, 1997; Klaassen, 1988; Mehta et al., 2020; Rao et al., 2008; Steiner & Smith, 1998) (see Supporting Information for details).

Geostationary Operational Environmental Satellite (GOES-16) imagery (Schmit et al., 2017) was used to identify the formation, evolution, phases of stratiform rainfall and vertical cloud development. The cloud-top brightness temperature (BT, $^{\circ}\text{C}$) values were extracted from the GOES-16 imagery in 10-minute intervals. The BT values were used to track the formation and evolution of stratiform rainfall before and during intra-events. The threshold BT values were used to indicate convective systems (BT lower than -38°C) and convective updrafts (cooling rates $>4^{\circ}\text{C}$) (Machado & Laurent, 2004; Ribeiro et al., 2019). The cloud area was calculated using GOES-16 BT and rain rates. The BT and rain rates were compared in the imagery to determine the number of pixels covering the sampling site (Figure S1). The quantity of pixels with a BT lower than 0°C and rain rates greater than 0 mm h^{-1} represents the stratiform cloud area. The number of pixels was then multiplied by the area of a single pixel ($2 \times 2 \text{ km}$), resulting in the cloud area being expressed in km^2 .

Total cloud ice and liquid water contents from ERA-5 reanalysis were used to characterize the cloud column water content during different stratiform rainfall stages. Liquid and ice contents were used as good predictors of stratiform rainfall stages (Zhang & Fu, 2018), due to their clear changes during the cloud's life cycle.

2.3 Identification of rainfall life stages and weather systems

The identification of rainfall systems based on BT variation from satellite and/or radar sources has been widely used in previous studies (Byers & Braham, 1949; Kumar et al., 2020; Machado et al., 1998; Mapes, 1993; Williams & R. A. Houze, 1987) (see Supporting Information for details). Based on previous studies by Byers and Braham (1949) and Kumar et al. (2020), the life cycle stages of the convective systems are defined and illustrated in Figure 1: a) the growing stage, characterized by decreasing BT values and increasing cloud area over time; b) the developed stage, when BT values remain constant during rainfall events; c) the dissipating stage, characterized by a gradual BT increase over time. Three hours prior to arrival over the study area were used to monitor the spatial and temporal movement of cloud systems. This time frame was chosen because stratiform rainfall typically forms within one to three hours (Houze, 1993).

The weather systems were defined according to the synoptic map and the meteorological technical bulletin of the Centre for Weather Forecasting and Climatic Studies of the National Institute for Space Research (CPTEC/INPE) (see Supporting Information for details).

2.4 Statistical tests

Statistical tests were performed to examine the correlation between isotopic parameters ($\delta^{18}\text{O}$, $\delta^2\text{H}$, and d -excess) as dependent variables and meteorological data (AWS and MRR) as independent variables (Table 1SM). All statistical tests at a significance level of 0.05 were performed using Rstudio (R Core Team, 2024). The analysis of variance (ANOVA, with F and p-value) was applied to test the statistical differences (p-value < 0.05) of isotopic parameters and meteorological data between events. Pearson correlations between isotopic parameters and meteorological variables from AWS and MRR (near-surface and higher altitude) were computed using the *corrplot* package in R (Taiyun Wei & Viliam, 2017).

3 Results

3.1 Meteorological and isotopic conditions

The meteorological and isotopic characteristics of stratiform rainfall events are summarized in Figure S2. In general, the stratiform rainfall events were described by low LCL (< 245 m), high RH (> 94 %), low ARR (< 0.2 mm min⁻¹), low LWC (< 0.6 g.m⁻³) and distinct patterns in T, Z, Rrr, w, LWC, duration, and BT (Figure S2). The longer event lasting 4 hours and 55 minutes exhibited the lowest $\delta^{18}\text{O}_{\text{mean}}$ (-12.4 ‰) and d -excess_(mean) (11.3 ‰). Variations in meteorological parameters were linked to the distinct mean isotopic composition (Figure S2). Higher $\delta^{18}\text{O}_{\text{mean}}$ (≥ -5.1 ‰) corresponded to lower RH values (≤ 95 %), higher Z (≥ 19 dBZ) and higher BT (≥ -23 °C), while events presenting with a lower $\delta^{18}\text{O}_{\text{mean}}$ (≤ -6.1 ‰) showed higher RH (≥ 95 %), lower Z (≤ 18 dBZ) and the lowest BT (≤ -44 °C).

The correlation between $\delta^{18}\text{O}$ -RH, $\delta^{18}\text{O}$, w, and Z at different altitudes was strong ($r \geq \pm 0.5$) and significant (p < 0.05) (Table S1). The best altitude range for correlations was 1.8 km to 7.7 km for w and 2.7 km to 9.8 km for Z. However, the correlations between isotopic composition and AWS, MRR meteorological variables were weaker ($r < 0.5$). Variable weather systems were responsible for the formation of the stratiform rainfall events (Table 1). The initial and mean isotopic composition of the trough and cold fronts is enriched compared to that of the South Atlantic Convergence Zone (SACZ), thermal instability, and low-pressure area (LPA) (Table 1).

3.2 Development of stratiform systems

Figures 2 illustrate the development of stratiform clouds. Growing stages were observed on 25 Sep 19 and 08 Oct 19 events, while developed stages was observed during other events (27 June 20, 05 Jan 20, 12 Dec 19, 10 Feb 20). Note that the growing stages were characterized by small clouds and fewer pixels in GOES-16 images, which were observed only at the start of isotope sampling (denoted with a red symbol in Figure 2, Panel a).

On 27 June 20, the edge of a cloud system passing over Rio Claro caused significant changes in BT between 3 to 1 hour before the event (Figure 2). At the beginning of isotope collection, the differences in BT values were reduced, indicating a more stable and developed stage for the cloud system (Panel b). Large conglomerates of unified clouds were observed on 05 Jan 20 (Panel b) and 10 Feb 20 (Panel c), while small and less homogeneous cloud shapes were recorded on 12 Dec 19 (Panel c). These stratiform events showed a greater spatial evolution (~200 km), causing slight variations in BT values before (3 hours) the start of isotope sampling, indicating a developed stage.

3.3 Cloud area and water content

The evolution of stratiform rainfall produced variations in cloud area and water content as detailed in Table 1. On the 25 Sep 19 and 08 Oct 19, the $\delta^{18}\text{O}_{\text{mean}}$ values were higher, cloud area and liquid-ice ratio were lower in relation to events on 05 Jan 20, 10 Dec 19, and 10 Feb 20. Note that on 10 Feb 20, the lowest $\delta^{18}\text{O}_{\text{mean}}$ (-12.4 ‰) coincided with extensive cloud coverage (108 km²) and a higher proportion of liquid-ice (13.9). In contrast, on 27 June 20, despite the low $\delta^{18}\text{O}_{\text{mean}}$ (-5.1‰) and high liquid-ice ratio (8.4), the smallest cloud area (24 km²) was observed.

3.4 Intra-event variations

Figure 3 shows the intra-events variability in isotopic compositions, BT (cloud stages), and the rainfall vertical profile. In general, $\delta^{18}\text{O}$ values decreased between the beginning and end of the events, except for the event on 10 Dec 2019, with the opposite trend. Intra-event temporal isotope patterns were characterized by V- (25 Sep 19), W- (08 Oct 19 and 27 June 20), L- (10 Feb 20), M- (10 Dec 19), and variable (05 Jan 20) shapes. Overall, *d*-excess temporal trends were opposite to those for $\delta^{18}\text{O}$.

On 25 Sep 19 (Figure 3a) and 08 Oct 19 (Figure 3b), cloud systems exhibited growth, development, and dissipation stages. On 05 Jan 20, there was a transition from the developed stage, characterized by smooth BT variations, to the dissipation stage, marked by a sharp increase in BT (Figure 3e). On 27 June 20, the dissipation stage was observed in most of the event (Figure 3f). Commonly, during the cloud dissipation stage, a new cloud formation causes a decrease in BT values. As a result of these cloud stage changes, both $\delta^{18}\text{O}$ and *d*-excess values exhibited notable changes within the events (Figure 3b,d,i,k).

The vertical structure of the fall velocity (*w*) was unique across the intra-events. During the growing stages on 25 Sep 19 and 08 Oct 19, the melting layer was variable (Figure 3c,d), with lower average heights and mean Rrr (Table 1). During the developed stages, only the event on 08 Oct 19 exhibited high values of *w* below the melting layer, corresponding to the most negative $\delta^{18}\text{O}$ value (-2.2‰) in the event (Figure 3b,d). The events on 05 Jan 20 and 27 June 20 showed a consolidated formation of the melting layer, with a variable average height (Table 1). The vertical structure was more pronounced, with higher values of *w* at the beginning of the events, resulting in the highest mean Rrr between the events (Table 1). The events on 10 Dec 19 and 10 Feb 20 presented the highest melting layer and lower Rrr (Table 1). Although the melting layers were high, they were not constant throughout the events. This was due to the interruptions in their formation caused by changes in the dissipation stages of the clouds and the entry of clouds with new characteristics (Figure 3k,l).

4 Weather systems and stratiform rainfall isotopic variability in the inland tropics of Brazil

The acting weather systems across the inland tropics in Brazil commonly generate two categories of stratiform events. A first group is characterized by shallow cloud-tops with BT values higher than -38 °C and small cloud area coverage (<36 km²). These cloud systems are formed by troughs and cold fronts. A second group associated with deep cloud systems and BT values lower than -38 °C and large cloud coverage (>48 km²). These events were caused by SACZ formation, thermal instability, and LPA (Table 1). In general, dynamic forcings such as troughs and cold fronts generate less vigorous cloud systems, while thermodynamic forcings such as SACZ, thermal instability, and LPA generate more vigorous cloud systems (Garreaud, 2000; Garreaud & Aceituno, 2007; Machado & Rossow, 1993; Reboita et al., 2010; Siqueira et

al., 2005; Siqueira & Machado, 2004). Synoptic forcings affect condensation, leading to rainfall and causing differences in isotopic composition between stratiform events.

Thus, the events with the largest cloud cover area and lowest BT (higher cloud-top) exhibited lower isotopic composition ($\delta^{18}\text{O}_{\text{initial}} \leq -4.2\text{‰}$ and $\delta^{18}\text{O}_{\text{mean}} \leq -6.1\text{‰}$, Table 1). The condensate becomes increasingly depleted as it condenses at higher altitudes. This is because the lower temperature causes the vapor to be more strongly depleted by previous condensation at higher altitudes (Celle-Jeanton et al., 2004; Gonfiantini et al., 2001). Smaller cloud coverage and higher BT values (lower cloud-top) produce condensation at lower altitudes. This results in less depletion of the vapor, denoted by enriched rainfall events ($\delta^{18}\text{O}_{\text{initial}} \geq -3.8\text{‰}$ and $\delta^{18}\text{O}_{\text{mean}} \geq -5.1\text{‰}$). Previous studies have found that $\delta^{18}\text{O}$ values decrease with increasing cloud top height and precipitation height in the troposphere, supporting these findings (S. Gedzelman et al., 2003; S. D. Gedzelman & Lawrence, 1990).

A secondary influence on the isotopic depletion between the events is the relationship between the cloud phases and the liquid-ice ratios. The liquid-ice ratio was greater in the more depleted events due to the generation of a larger condensed phase. Therefore, residual water vapor and cloud water are depleted, and heavy isotopes are preferentially removed by Rayleigh distillation (Rozanski & Sonntag, 1982). The melting layer height contains information about how stratiform cloud systems form. It integrates information about the height of condensation and cloud formation process and phases along the trajectory before reaching the observation site. Additionally, it provides information on the transition of the convective-stratiform fraction and changes in microphysical processes up to the fusion in the melting layer and the formation of raindrops. The most depleted events exhibited higher average melting layers (≥ 3.8 km) compared to the most enriched events with average heights of ≤ 3.6 km (Table 1). This relationship between higher melting layer and lower isotopic composition is supported by previous studies (Hu et al., 2022; C. Risi et al., 2019), and strong and significant statistical correlations between $\delta^{18}\text{O}$, w and Z at altitude for all events (Table S1).

5 Key drivers in controlling intra-event stratiform isotopic variability

During intra-events, isotopic variations are controlled by microphysical processes. These processes are characterized by the formation of ice particles near the top of the clouds. The ice particles grow initially by vapor deposition (diffusion) and later by aggregation. They slowly fall towards the surface until the melting layer is formed (Aggarwal et al., 2016; Houze, 1993, 1997). The observation of microphysical processes throughout the events allowed for examining the evolution of the stratiform cloud system between phases and its impact on the formation of the fusion layer, as demonstrated by the BT values and vertical profile of w . Different phases of the cloud system were observed, resulting in either consolidated formation of the melting layer or inconsistent melting layer formation (Figure 3). During the growing and developing phases of the cloud system, microphysical processes produced consolidated melting layers, vertical w profiles with higher values, and higher mean Rrr values. This led to a decrease in $\delta^{18}\text{O}$ values, with the most significant depletion occurring in some events. Unconsolidated melting layers may form during the dissipating phase and/or entry of a new cloud, causing a decrease in the vertical values of w and resulting in lower mean Rrr values. These transition phases caused the change in the patterns of isotopic variation during intra-events, explained the diversity of isotopic shapes observed between the stratiform events.

6 Conclusions

Refining the analysis outside of the seasonal context in previous studies, based on the high-frequency isotopic composition of rainfall, allowed for a better understanding of the large variability of $\delta^{18}\text{O}$ and d -excess, and their relation to regional and local atmospheric influences. Regional and local influences drive the observed isotopic variability. These factors were evaluated to explain the isotopic variations among events and during intra-events (trend and shape of variations).

Regional influences are linked to atmospheric systems that create shallow ($\text{BT} \geq -38^\circ\text{C}$) and deep cloud systems ($\text{BT} \leq -38^\circ\text{C}$). These systems control the degree of depletion between stratiform events. Cloud systems formed far (~ 200 km) from Rio Claro had more time to grow and develop. This resulted in higher cloud-top, cloud area, and liquid-ice ratios. Thus, there was a greater depletion in heavy isotopes due to Rayleigh distillation than the stratiform events formed near Rio Claro. Due to the shorter time frame for growth and development, the BT values were higher, with lower cloud top, cloud area, and liquid-ice ratios, resulting in a minor degree of depletion. This mechanism is evident across a wide range of isotopic compositions between events.

The local aspects of rainfall were explained by BT values (hence cloud phases) and the vertical structure of rainfall during intra-events. The microphysical processes of stratiform formation change according to the phase of the systems (transitions between growth, development, dissipation, and entry of new clouds), producing variations in the isotopic composition. Thus, the isotopic composition of the stratiform rainfall during the intra-events reflects the local microphysical changes that occurred during the phase transition of the cloud system, which changed its pattern of isotopic variation during the events and resulted in a varied isotopic shape between events.

Our study reveals that for the inland tropical regions, where fewer high-frequency studies have been carried out, multiple regional and local factors need to be considered when assessing rainfall isotope variability. Finally, we emphasize the need to use high frequency in future studies across the tropics to advance isotopic interpretations and improve model parametrization based on robust surface isotope observations.

Acknowledgments

This work was funded by grants the São Paulo Research Foundation (FAPESP) under Processes 2018/06666-4 and by the International Atomic Energy Agency Grant CRP-F31006. The first author acknowledges FAPESP (Process 2019/03467-3 and 2021/10538-4) and National Council for Scientific and Technological Development (CNPq) (Process 383633/2022-2) for the scholarship provided.

Open Research

The complete dataset with isotopes ratios and meteorological parameters can be found in the Mendeley Data repository at: (<https://data.mendeley.com/datasets/kk3gs8zn4s/1>). Data from GOES-16 and ERA-5 reanalysis are publicly available at: (https://home.chpc.utah.edu/~u0553130/Brian_Blaylock/cgi-bin/goes16_download.cgi) and

(<https://cds.climate.copernicus.eu/cdsapp#!/search?type=dataset>). The synoptic map is available at (<https://www.marinha.mil.br/chm/dados-do-smm-cartas-sinoticas/cartas-sinoticas>). The MRR, GOES-16, and ERA-5 reanalysis data were processed using the Python language (Python Software Foundation, 2024).

References

- Aemisegger, F. ., Spiegel, J. K. ., Pfahl, S. ., Sodemann, H. ., Eugster, W. ., & Wernli, H. (2015). Isotope meteorology of cold front passages: A case study combining observations and modeling. *Geophysical Research Letters*, 42(13), 5652–5660. <https://doi.org/10.1002/2015GL063988>
- Aggarwal, P. K., Romatschke, U., Araguas-Araguas, L., Belachew, D., Longstaffe, F. J., Berg, P., et al. (2016). Proportions of convective and stratiform precipitation revealed in water isotope ratios. *Nature Geoscience*, 9(8), 624–629. <https://doi.org/10.1038/ngeo2739>
- Byers, H. R., & Braham, R. R. (1949). *Thunderstorms and the Thunderstorm Project. Report of the Thunderstorm Project. U.S. Government Printing Office.*
- Celle-Jeanton, H., Travi, Y., & Blavoux, B. (2001). Isotopic typology of the precipitation in the Western Mediterranean Region at three different time scales. *Geophysical Research Letters*, 28(7), 1215–1218. <https://doi.org/10.1029/2000GL012407>
- Celle-Jeanton, H., Gonfiantini, R., Travi, Y. & Sol, B. (2004). Oxygen-18 variations of rainwater during precipitation: application of the Rayleigh model to selected rainfalls in Southern France. *Journal of Hydrology*, 289(1–4), 165–177. <https://doi.org/10.1016/j.jhydrol.2003.11.017>
- Dansgaard, W. (1964). Stable isotopes in precipitation. *Tellus*, 16(4), 436–468. <https://doi.org/10.3402/tellusa.v16i4.8993>
- Endries, J. L., Perry, L. B., Yuter, S. E., Seimon, A., Andrade-Flores, M., Winkelmann, R., et al. (2018). Radar-observed characteristics of precipitation in the tropical high andes of Southern Peru and Bolivia. *Journal of Applied Meteorology and Climatology*, 57(7), 1441–1458. <https://doi.org/10.1175/JAMC-D-17-0248.1>
- Froehlich, K., Gibson, J. J., & Aggarwal, P. (2002). Deuterium excess in precipitation and its climatological significance. *Journal of Geophysical Research-Atmospheres*, (July 2002), 1–23.
- García-Santos, S., Sánchez-Murillo, R., Peña-Paz, T., Chirinos-Escobar, M. J., Hernández-Ortiz, J. O., Mejía-Escobar, E. J., & Ortega, L. (2022). Water stable isotopes reveal a complex rainfall to groundwater connectivity in central Honduras. *Science of the Total Environment*, 844(June). <https://doi.org/10.1016/j.scitotenv.2022.156941>
- Garreaud, R. D. (2000). Cold air incursions over subtropical South America: Mean structure and dynamics. *Monthly Weather Review*, 128(7 II), 2544–2559. [https://doi.org/10.1175/1520-0493\(2000\)128<2544:caioss>2.0.co;2](https://doi.org/10.1175/1520-0493(2000)128<2544:caioss>2.0.co;2)
- Garreaud, R. D., & Aceituno, P. (2007). Atmospheric Circulation and Climatic Variability. *The Physical Geography of South America*, 45–59.

- Gedzelman, S., Lawrence, J., Gamache, J., Black, M., Hindman, E., Black, R., et al. (2003). Probing hurricanes with stable isotopes of rain and water vapor. *Monthly Weather Review*, 131(6), 1112–1127. [https://doi.org/10.1175/1520-0493\(2003\)131<1112:PHWSIO>2.0.CO;2](https://doi.org/10.1175/1520-0493(2003)131<1112:PHWSIO>2.0.CO;2)
- Gedzelman, S. D., & Lawrence, J. R. (1990). The Isotopic Composition of Precipitation from Two Extratropical Cyclones. *American Meteorological Society*, 118, 495–509. [https://doi.org/10.1175/1520-0493\(1990\)118,0495: TICOPF.2.0.CO;2](https://doi.org/10.1175/1520-0493(1990)118,0495: TICOPF.2.0.CO;2)
- Gonfiantini, R., Roche, M.-A., Olivry, J.-C., Fontes, J.-C., & Zuppi, G. M. (2001). The altitude effect on the isotopic composition of tropical rains. *Chemical Geology*, 181(1–4), 147–167. [https://doi.org/10.1016/S0009-2541\(01\)00279-0](https://doi.org/10.1016/S0009-2541(01)00279-0)
- Graf, P., Wernli, H., Pfahl, S., & Sodemann, H. (2019). A new interpretative framework for below-cloud effects on stable water isotopes in vapour and rain. *Atmospheric Chemistry and Physics*, 19(2), 747–765. <https://doi.org/10.5194/acp-19-747-2019>
- Han, T., Zhang, M., Wang, S., Qu, D., & Du, Q. (2020). Sub-hourly variability of stable isotopes in precipitation in the marginal zone of East Asian monsoon. *Water (Switzerland)*, 12(8). <https://doi.org/10.3390/W12082145>
- Han, X., Lang, Y., Wang, T., Liu, C.-Q., Li, F., Wang, F., et al. (2021). Temporal and spatial variations in stable isotopic compositions of precipitation during the typhoon Lekima (2019), China. *Science of The Total Environment*, 762, 143143. <https://doi.org/10.1016/j.scitotenv.2020.143143>
- Houze, R. A. J. (1989). Observed structure of mesoscale convective systems and implications for large-scale heating. *Quart. J. Roy. Meteor. Soc.*, 115, 425–461.
- Houze, R. A. J. (1993). *Cloud dynamics*. Cloud dynamics. Academic Press Limited. [https://doi.org/10.1016/0377-0265\(87\)90017-0](https://doi.org/10.1016/0377-0265(87)90017-0)
- Houze, R. A. J. (1997). Stratiform precipitation in regions of convection: A Meteorological Paradox? *Bulletin of the American Meteorological Society*, 78, 2179–2195.
- Hu, J., Bailey, A., Nusbaumer, J., Dee, S., Sasser, C., & Worden, J. (2022). Tracking shallow convective mixing and its influence on Low-level clouds with stable water isotopes in vapor. *Journal of Geophysical Research: Atmospheres*, 127(5). <https://doi.org/10.1029/2021JD035355>
- Jouzel, J., Delaygue, G., Landais, A., Masson-Delmotte, V., Risi, C., & Vimeux, F. (2013). Water isotopes as tools to document oceanic sources of precipitation. *Water Resources Research*, 49(11), 7469–7486. <https://doi.org/10.1002/2013WR013508>
- Klaassen, W. (1988). Radar Observations and Simulation of the Melting Layer of Precipitation. *Journal of the Atmospheric Sciences*, 45(24), 3741–3753.
- Kumar, S., Castillo-Velarde, C. Del, Flores Rojas, J. L., Moya-Álvarez, A., Martínez Castro, D., Srivastava, S., & Silva, Y. (2020). Precipitation structure during various phases the life cycle of precipitating cloud systems using geostationary satellite and space-based precipitation radar over Peru. *GIScience and Remote Sensing*, 57(8), 1057–1082. <https://doi.org/10.1080/15481603.2020.1843846>

- Landais, A., Risi, C., Bony, S., Vimeux, F., Descroix, L., Falourd, S., & Bouygues, A. (2010). Combined measurements of $\delta^{18}\text{O}$ excess and d-excess in African monsoon precipitation: Implications for evaluating convective parameterizations. *Earth and Planetary Science Letters*, 298(1–2), 104–112. <https://doi.org/10.1016/j.epsl.2010.07.033>
- Machado, L. A. T., & Laurent, H. (2004). The Convective System Area Expansion over Amazonia and Its Relationships with Convective System Life Duration and High-Level Wind Divergence. *Monthly Weather Review*, 132(3), 714–725. [https://doi.org/10.1175/1520-0493\(2004\)132<0714:TCSAEO>2.0.CO;2](https://doi.org/10.1175/1520-0493(2004)132<0714:TCSAEO>2.0.CO;2)
- Machado, L. A. T., & Rossow, W. B. (1993). Structural Characteristics and Radiative Properties of Tropical Cloud Clusters. *Monthly Weather Review*, 121, 3234–3260.
- Machado, L. A. T., Rossow, W. B., Guedes, R. L., & Walker, A. W. (1998). Life cycle variations of mesoscale convective systems over the Americas. *Monthly Weather Review*, 126(6), 1630–1654. [https://doi.org/10.1175/1520-0493\(1998\)126<1630:LCVOMC>2.0.CO;2](https://doi.org/10.1175/1520-0493(1998)126<1630:LCVOMC>2.0.CO;2)
- Mapes, B. E. R. A. H. (1993). Cloud clusters and superclusters over the oceanic warm pool. *Monthly Weather Review*, 121, 1398–1416.
- Mehta, S., Mehta, S. K., Singh, S., Mitra, A., Ghosh, S. K., & Raha, S. (2020). Characteristics of the Z–R Relationships Observed Using Micro Rain Radar (MRR-2) over Darjeeling (27.05° N, 88.26° E): A Complex Terrain Region in the Eastern Himalayas. *Pure and Applied Geophysics*, 177(9), 4521–4534. <https://doi.org/10.1007/s00024-020-02472-6>
- Muller, C. L., Baker, A., Fairchild, I. J., Kidd, C., & Boomer, I. (2015). Intra-Event Trends in Stable Isotopes: Exploring Midlatitude Precipitation Using a Vertically Pointing Micro Rain Radar. *Journal of Hydrometeorology*, 16(1), 194–213. <https://doi.org/10.1175/JHM-D-14-0038.1>
- Munksgaard, N. C., Kurita, N., Sánchez-Murillo, R., Ahmed, N., Araguas, L., Balachew, D. L., et al. (2019). Data Descriptor: Daily observations of stable isotope ratios of rainfall in the tropics. *Scientific Reports*, 9(1), 1–7. <https://doi.org/10.1038/s41598-019-50973-9>
- Munksgaard, N. C., Zwart, C., Haig, J., Cernusak, L. A., & Bird, M. I. (2020). Coupled rainfall and water vapour stable isotope time series reveal tropical atmospheric processes on multiple timescales. *Hydrological Processes*, 34(1), 111–124. <https://doi.org/10.1002/hyp.13576>
- Python Software Foundation. (2024). Python Language Reference, version 3.7. <http://www.python.org/>.
- R Core Team. (2024). A language and environment for statistical computing. R Foundation for Statistical Computing, Vienna, Austria. <https://www.R-project.org/>.
- Rao, N. T., Kirankumar, N. V. P., Radhakrishna, B., & Rao, N. D. (2008). Classification of tropical precipitating systems using wind profiler spectral moments. Part I: Algorithm description and validation. *Journal of Atmospheric and Oceanic Technology*, 25(6), 884–897. <https://doi.org/10.1175/2007JTECHA1031.1>

- Reboita, M. S., Gan, M. A., Rocha, R. P. da, & Ambrizzi, T. (2010). Regimes de precipitação na América do Sul: uma revisão bibliográfica. *Revista Brasileira de Meteorologia*, 25(2), 185–204. <https://doi.org/10.1590/S0102-77862010000200004>
- Ribeiro, B. Z., Machado, L. A. T., Biscaro, T. S., Freitas, E. D., Mozer, K. W., & Goodman, S. J. (2019). An evaluation of the GOES-16 rapid scan for nowcasting in southeastern Brazil: Analysis of a severe hailstorm case. *Weather and Forecasting*, 34(6), 1829–1848. <https://doi.org/10.1175/WAF-D-19-0070.1>
- Risi, C., Galewsky, J., Reverdin, G., & Briant, F. (2019). Controls on the water vapor isotopic composition near the surface of tropical oceans and role of boundary layer mixing processes. *Atmospheric Chemistry and Physics*, 19(19), 12235–12260. <https://doi.org/10.5194/acp-19-12235-2019>
- Risi, Camille, Bony, S., Vimeux, F., Chongd, M., & Descroix, L. (2010). Evolution of the stable water isotopic composition of the rain sampled along Sahelian squall lines. *Quarterly Journal of the Royal Meteorological Society*, 136(SUPPL. 1), 227–242. <https://doi.org/10.1002/qj.485>
- Rozanski, K., & Sonntag, C. (1982). Vertical distribution of deuterium in atmospheric water vapour. *Tellus*, 34(2), 135–141. <https://doi.org/10.3402/tellusa.v34i2.10795>
- Sánchez-Murillo, R., Durán-Quesada, A. M., Esquivel-Hernández, G., Rojas-Cantillano, D., Birkel, C., Welsh, K., et al. (2019). Deciphering key processes controlling rainfall isotopic variability during extreme tropical cyclones. *Nature Communications*, 10(1). <https://doi.org/10.1038/s41467-019-12062-3>
- Schumacher, C., & Houze, R. A. (2003). Stratiform rain in the tropics as seen by the TRMM precipitation radar. *Journal of Climate*, 16(11), 1739–1756. [https://doi.org/10.1175/1520-0442\(2003\)016<1739:SRITTA>2.0.CO;2](https://doi.org/10.1175/1520-0442(2003)016<1739:SRITTA>2.0.CO;2)
- Siqueira, J. R., & Machado, L. A. T. (2004). Influence of the frontal systems on the day-to-day convection variability over South America. *Journal of Climate*, 17(9), 1754–1766. [https://doi.org/10.1175/1520-0442\(2004\)017<1754:IOTFSO>2.0.CO;2](https://doi.org/10.1175/1520-0442(2004)017<1754:IOTFSO>2.0.CO;2)
- Siqueira, J. R., Rossow, W. B., Machado, L. A. T., & Pearl, C. (2005). Structural characteristics of convective systems over South America related to cold-frontal incursions. *Monthly Weather Review*, 133(5), 1045–1064. <https://doi.org/10.1175/MWR2888.1>
- Srivastava, R., Ramesh, R., & Rao, T. N. (2012). Relationship between stable isotope ratios and drop size distribution in tropical rainfall. *Journal of Atmospheric Chemistry*, 69(1), 23–31. <https://doi.org/10.1007/s10874-012-9227-4>
- Steiner, M., & Smith, J. A. (1998). Convective versus stratiform rainfall: An ice-microphysical and kinematic conceptual model. *Atmospheric Research*, 47–48, 317–326. [https://doi.org/10.1016/S0169-8095\(97\)00086-0](https://doi.org/10.1016/S0169-8095(97)00086-0)
- Sun, C., Shanahan, T. M., & Partin, J. (2019). Controls on the Isotopic Composition of Precipitation in the South-Central United States. *Journal of Geophysical Research: Atmospheres*, 124(14), 8320–8335. <https://doi.org/10.1029/2018JD029306>
- Taiyun Wei, & Viliam, S. (2017). R package “corrplot.” *Github*. <https://github.com/taiyun/corrplot>.

- Tremoy, G., Vimeux, F., Soumana, S., Souley, I., Risi, C., Favreau, G., & Oï, M. (2014). Clustering mesoscale convective systems with laser-based water vapor $\delta^{18}\text{O}$ monitoring in Niamey (Niger). *Journal of Geophysical Research: Atmospheres*, 119(9), 5079–5103. <https://doi.org/10.1002/2013JD020968>
- Williams, M. ., & R. A. Houze. (1987). Satellite-observed characteristics of winter monsoon cloud clusters. *Monthly Weather Review*, 115, 505–519. [https://doi.org/https://doi.org/10.1175/1520-0493\(1987\)115%3C0505:SOCOWM%3E2.0.CO;2](https://doi.org/https://doi.org/10.1175/1520-0493(1987)115%3C0505:SOCOWM%3E2.0.CO;2)
- Xu, T., Sun, X., Hong, H., Wang, X., Cui, M., Lei, G., et al. (2019). Stable isotope ratios of typhoon rains in Fuzhou, Southeast China, during 2013–2017. *Journal of Hydrology*, 570(January), 445–453. <https://doi.org/10.1016/j.jhydrol.2019.01.017>
- Zhang, A., & Fu, Y. (2018). Life cycle effects on the vertical structure of precipitation in East China measured by Himawari-8 and GPM DPR. *Monthly Weather Review*, 146(7), 2183–2199. <https://doi.org/10.1175/MWR-D-18-0085.1>

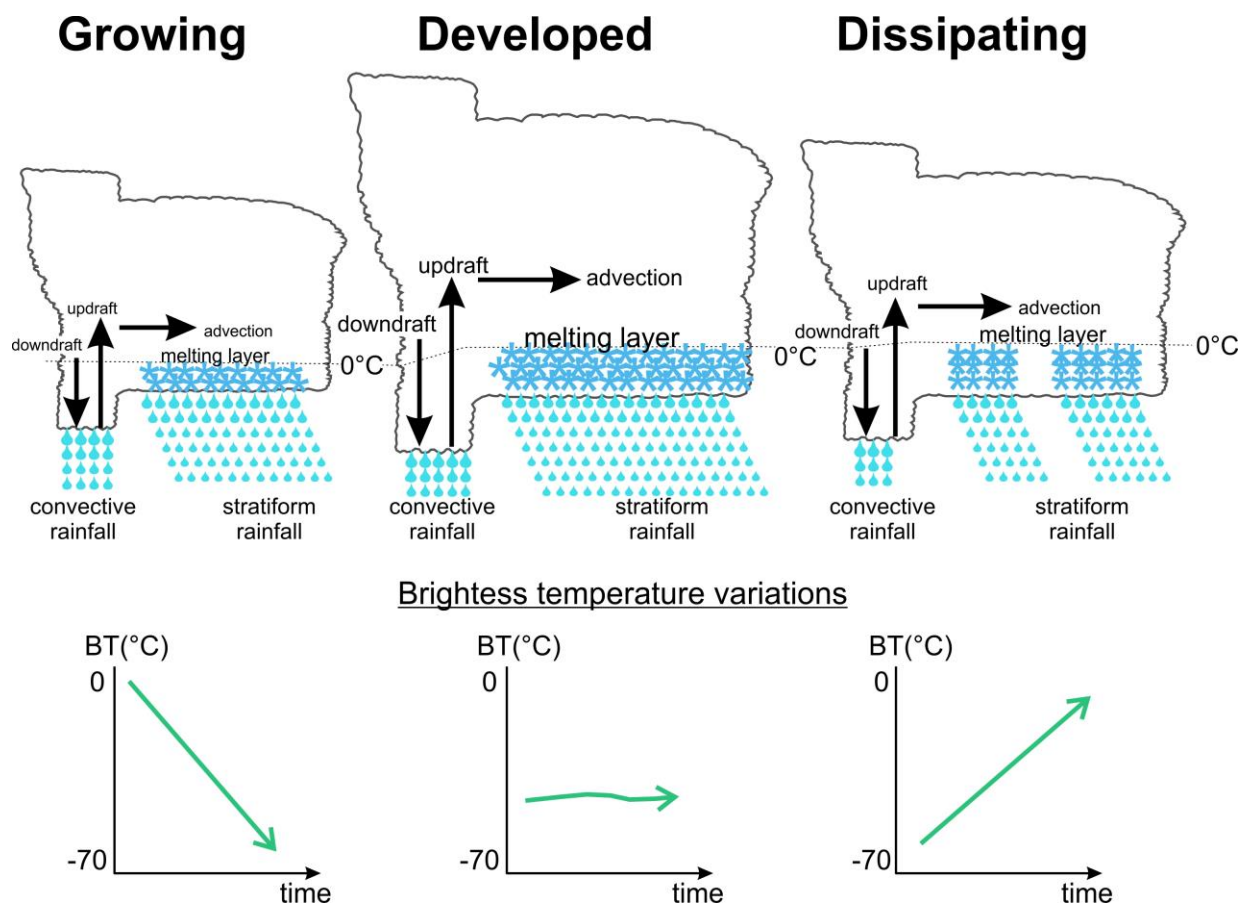


Figure 1. Conceptual diagram of tropical cloud system stages, including growing, developed, and dissipating phases with corresponding brightness temperature (BT) variations (decreasing, increasing, and constant values).

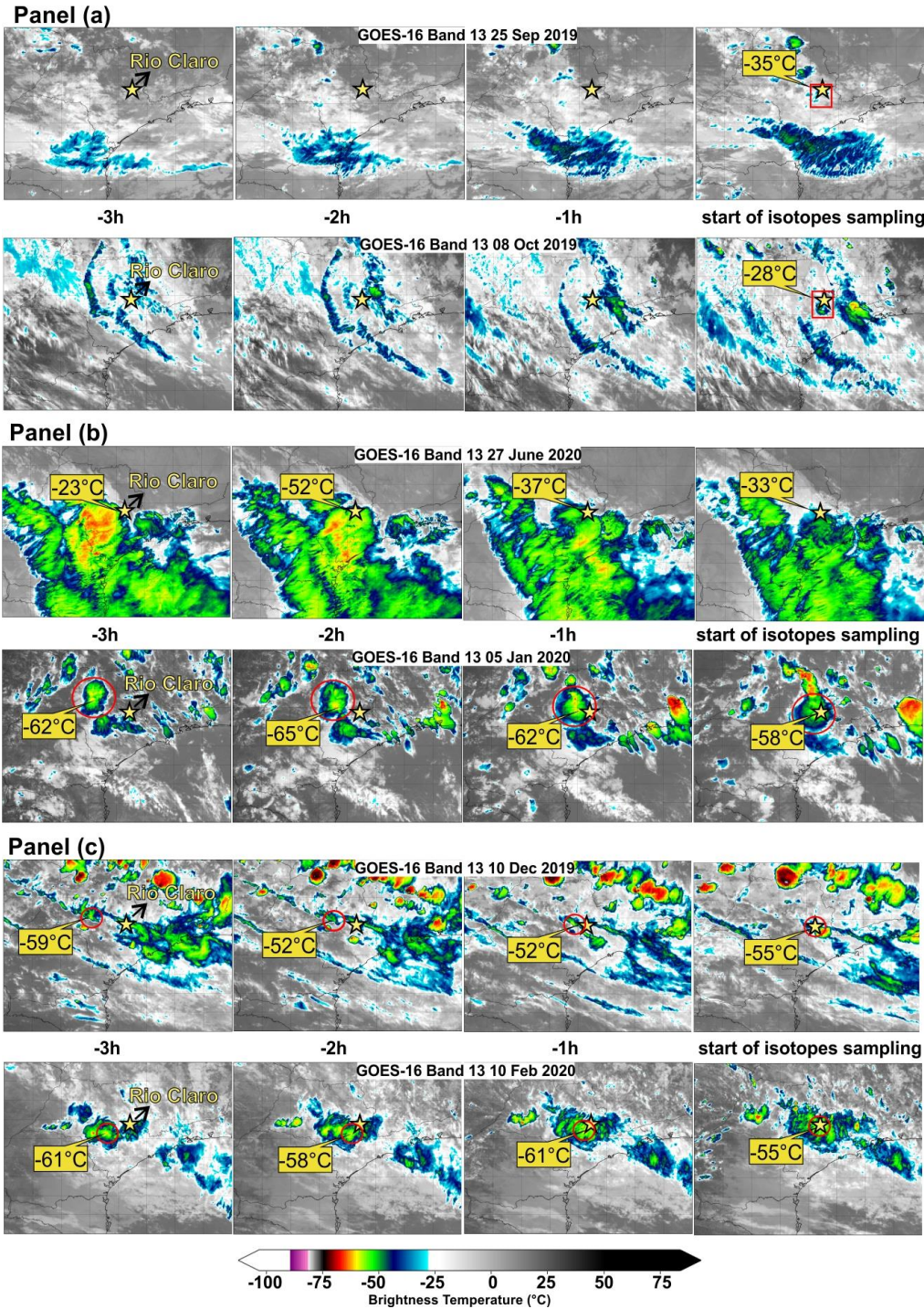
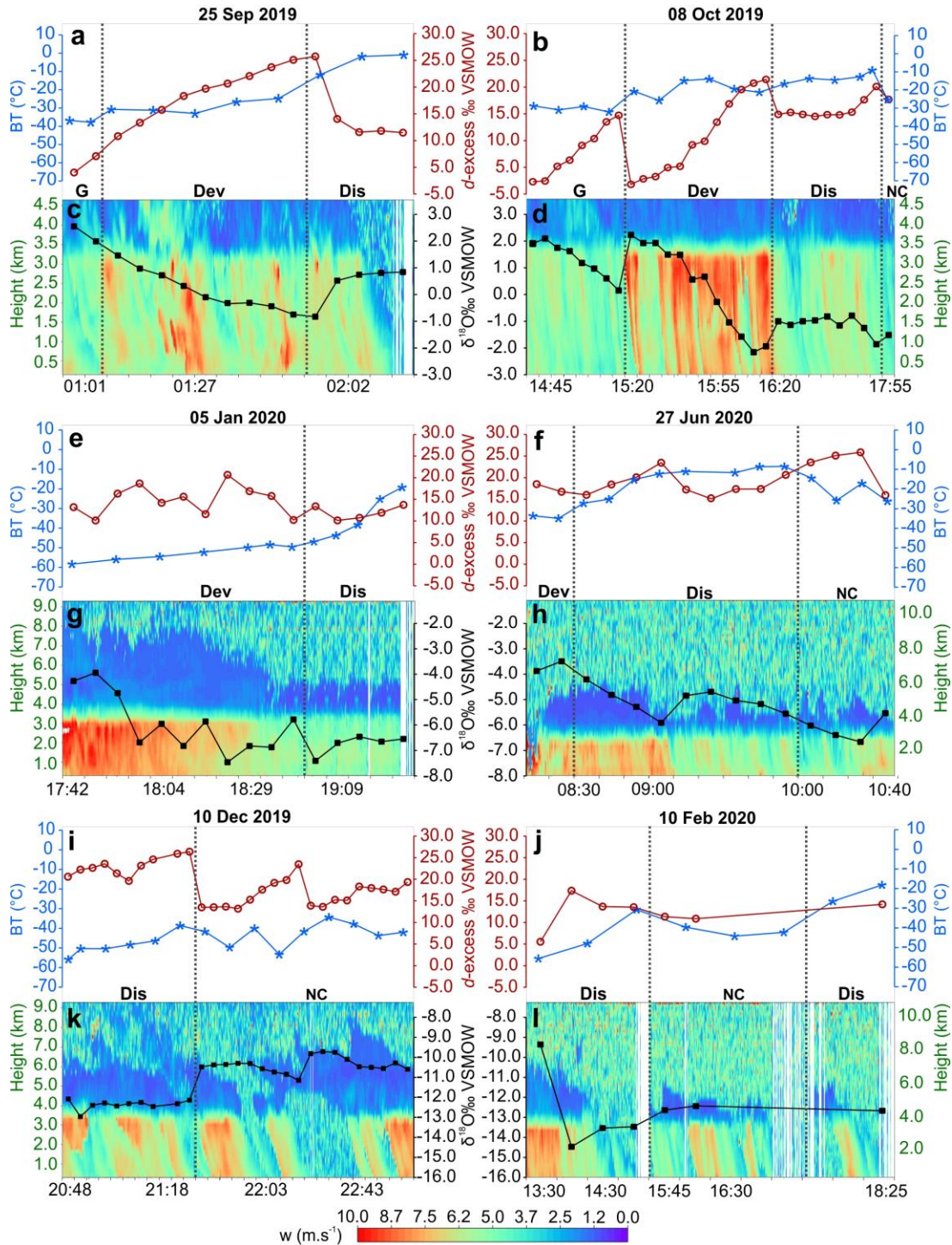


Figure 2. Sequence of GOES-16 satellite imagery frames from -3 hours, -2 hours, and -1 hour before rainfall in Rio Claro and from the start isotope collection. The yellow label shows the lower BT values from the center of the cloud system that passed over the Rio Claro site (yellow star).

501



502

503

504

505

506

507

Figure 3. Temporal variations of isotopic composition, cloud-top, and vertical structure of stratiform rainfall. The cloud top is illustrated by the trends of BT and the vertical structure of the precipitation by the profile of the fall velocity (w). G = growing phase; Dev = developing phase; Dis = dissipating phase; and NC = new cloud system with a BT increase of at least 4 °C, indicating updraft convection.

508 **Table 1.** Overview of weather systems, cloud features, meteorological and isotopic values.

Events	Weather system	$\delta^{18}\text{O}$ (‰)		d -excess (‰)		BT (°C)	cloud area (km ²)	liquid- ice ratio	Height of melting layer (km)	Rrr (mm min ⁻¹)
		initial	mean	initial	mean	start rainfall		mean	average	mean
25 September 2019	Trough	2.5	0.51	4.0	15.9	-35	28	1.4	3.4	2.0
08 October 2019	Cold front	1.6	-0.08	0.1	11.3	-28	36	0.8	3.6	1.7
27 June 2020	Cold front	-3.8	-5.1	18.3	19.2	-33	24	8.1	3.6	3.0
05 January 2020	SACZ	-4.2	-6.1	13.1	13.9	-58	104	0.5	3.1	4.1
10 December 2019	Thermal instability	-11.4	-10.7	20.8	18.8	-55	48	3.1	3.9	3.8
10 February 2020	LPA	-8.9	-12.4	4.9	11.3	-55	108	13.9	1.0	2.0

509 BT: brightness temperature; Rrr: rain rates of micro rain radar